⌘ *Author's Choice*

THE JOURNAL OF BIOLOGICAL CHEMISTRY VOL. 286, NO. 6, pp. 4072–4080, February 11, 2011


# Proteomic Characterization of Plasma Membrane-proximal T Cell Activation Responses*[S]

Received for publication, July 19, 2010, and in revised form, November 9, 2010 Published, JBC Papers in Press, December 2, 2010, DOI 10.1074/jbc.M110.165415

**Ben de Wet[‡], Tobias Zech[§], Mogjiborahman Salek[‡], Oreste Acuto[‡], and Thomas Harder[‡1]**

*From the [‡]Sir William Dunn School of Pathology, University of Oxford, Oxford OX1 3RE and the [§]Beatson Institute for Cancer Research, Glasgow G61 1BD, Scotland, United Kingdom*

**Early downstream responses of T lymphocytes following T cell antigen receptor (TCR) activation are mediated by protein complexes that assemble in domains of the plasma membrane. Using stable isotope labeling with amino acids in cell culture and mass spectrometry, we quantitatively related the proteome of αCD3 immunoisolated native TCR signaling plasma membrane domains to that of control plasma membrane fragments not engaged in TCR signaling. Proteins were sorted according to their relative enrichment in isolated TCR signaling plasma membrane domains, identifying a complex protein network that is anchored in the vicinity of activated TCR. These networks harbor widespread mediators of plasma membrane-proximal T cell activities, including propagation, balancing, and attenuation of TCR signaling, immune synapse formation, as well as cytoskeletal arrangements relative to TCR activation clusters. These results highlight the unique potential of systematic characterizations of plasma membrane-proximal T cell activation proteome in the context of its native lipid bilayer platform.**

T cell activation is triggered by T cell antigen receptor (TCR)[2] signals that are induced by its interaction with a cognate peptide-MHC (pMHC) presented on the surface of an antigen-presenting cell or target cell. The resulting tight conjugation zone between T cell and cognate cell is termed the immunological synapse (IS). Early signals are mediated by TCR signaling microclusters that form at the contact between a T cell and a pMHC-bearing membrane (1). These microclusters are transported centripetally and, at the center of the IS, form a plasma membrane domain called the central supramolecular activation cluster where early TCR signaling reactions are terminated (2). The peripheral supramolecular activation cluster surrounds the central supramolecular activation cluster and is marked by accumulation of LFA-1 paired with ICAM1 on the antigen-presenting cell surface (3).

An intact actin cytoskeleton is required for adhesion of T cells to pMHC-bearing surfaces and supports initial formation of TCR-signaling microclusters (1). Actin-rich lamellipodia form at the periphery of the IS at the contact between a cognate target cell and activated cytolytic T lymphocyte (CTL), although central regions of the IS are depleted of actin, freeing the way for the secretion of lytic granules into the synaptic cleft (4). Actin-rich rings also surround the contact of Jurkat T cells with a glass coverslip coated with TCR-activating αCD3 antibodies, although actin filaments are depleted from the central zone of contact to the coverslip (5).

Jurkat T cells polarize their microtubules toward αCD3 antibody-coated beads (6), recapitulating the rearrangement of the microtubule cytoskeleton of activated T lymphocytes critical for physiological effector functions. Lytic granules of CTLs are transported along microtubules and accumulate at the microtubule organizing center. Following activation of CTLs, the microtubule organizing center closely associates with the plasma membrane facing the IS, ensuring that lytic granules are effectively discharged toward the target cell (4).

TCR signaling commences with phosphorylation of cytoplasmic immunoreceptor tyrosine-based activation motifs in the CD3 subunits of the TCR complex by the membrane-anchored src family tyrosine kinases, LCK and FYN (7). Phosphorylated immunoreceptor tyrosine-based activation motifs recruit the cytosolic tyrosine kinase, ZAP-70, which in turn phosphorylates a defined set of tyrosines on the cytoplasmic domains of the transmembrane scaffolding protein, linker for activation of T cells (LAT). Phosphotyrosine motifs of LAT consequently bind the SH2 domain-containing adaptors, GADS and GRB2, and the signaling enzyme PLCγ to mediate early T cell activation reactions (8).

We have established a procedure to biochemically isolate native T cell plasma membrane domains engaged in TCR signaling. Western blots of these isolates demonstrated tyrosine phosphorylation-dependent assembly of a cooperative LAT-nucleated network of signaling proteins in plasma membrane domains in the vicinity of activated TCR (9, 10). Here, we extended this approach by employing stable isotope labeling with amino acids in cell culture (SILAC) and mass spectrometry to characterize plasma membrane-proximal protein networks mediating TCR activation responses. The important

* This work was supported by Wellcome Trust Project Grant 082782/2/07/2.
[S] The on-line version of this article (available at http://www.jbc.org) contains supplemental Tables 1 and 2.
⌘ *Author's Choice*—Final version full access.
[1] Recipient of support from the Edward Penley Abraham Trust. To whom correspondence should be addressed: South Parks Rd., Oxford OX1 3RE, United Kingdom. Tel.: 44-1865-285690; Fax: 44-1865-275515; E-mail: thomas.harder@path.ox.ac.uk.
[2] The abbreviations used are: TCR, T cell antigen receptor; SILAC, stable isotope labeling with amino acids in cell culture; pMHC, peptide-MHC; CTL, cytolytic T lymphocyte; LAT, linker for activation of T cell; αTfR, anti-transferrin receptor; IS, immunological synapse; SH, Src homology; PLCγ, phospholipase Cγ; H, heavy; L, light; GO, Gene Ontology; GEF, GDP/GTP exchange factor.

potential of mass spectrometry-based proteomics in cell biology is excellently reviewed in Ref. 11.

## EXPERIMENTAL PROCEDURES

*Antibodies and Reagents*—α-Transferrin receptor antibody (B3/25) and α-CD3ϵ antibody (OKT3) were purified from hybridoma culture supernatants. α-Phosphotyrosine antibodies (PY99) were obtained from Santa Cruz Biotechnology. α-LAT polyclonal rabbit antiserum was obtained from Upstate; α-Crk antibody was from BD Biosciences; α-Alix antibody was from Santa Cruz Biotechnology. IRDye 800CW-conjugated α-mouse IgG and IRDye 680CW-conjugated α-rabbit IgG were from LICOR Biosciences. M-450 goat anti-mouse IgG Dynabeads were obtained from Invitrogen and coated with 3.3 μg of antibody per $10^7$ beads in the presence of 1% immunoglobulin-free bovine serum albumin (Sigma).

*Bead Stimulation and Western Blotting*—Jurkat T cells were conjugated with an equal amount of antibody-coated beads or left untreated for 5 min on ice and subsequently heated to 37 °C for 3 min. Reactions were stopped by adding 1 ml of ice-cold H-buffer (250 mM sucrose, 10 mM HEPES, pH 7.2, 2 mM $MgCl_2$, 10 mM NaF. and 1 mM pervanadate), and cell pellets were lysed in SDS-PAGE loading buffer. Lysates equivalent to $10^5$ cells or immunoisolates from $5 \times 10^7$ cells were loaded onto precast 4–12% NuPAGE SDS gels (Invitrogen), and following electrophoresis, proteins were transferred to HybondC membranes (Amersham Biosciences) by semidry blotting using a Bio-Rad Trans-blot apparatus. Immunoreactive bands were visualized by infrared fluorescence detection using a LICOR Odyssey detection system.

*SILAC*—Custom L-arginine- and L-lysine-deficient RPMI 1640 medium (Pierce) was supplemented with 10% dialyzed fetal bovine serum (Invitrogen), 100 mg/liter penicillin (PAA Laboratories), and 100 mg/liter streptomycin (PAA Laboratories). Heavy medium was additionally supplemented with 62.5 mg/liter L-[$^{13}C_6$,$^{15}N_4$]arginine·HCl (Cambridge Isotope Laboratories) and 50 mg/liter L-[$^{13}C_6$,$^{15}N_2$]lysine·2HCl (Cambridge Isotope Laboratories), and light medium was supplemented with identical quantities of corresponding unlabeled amino acids (Sigma). Jurkat T cells were cultivated in heavy or light medium, respectively, at 37 °C in a humidified atmosphere containing 5% $CO_2$ for at least six cell doublings. Heavy isotope-labeled cultures were used for stimulation and light isotope-labeled cultures for nonstimulated control experiments.

*Immunoisolation*—Immunoisolation of activated cell membrane patches was performed as described previously (12). Briefly, cells were harvested from culture media, washed with HEPES-buffered RPMI 1640 medium containing 1% immunoglobulin-free bovine serum albumin, and conjugated with Dynabeads on ice for 5 min. Conjugates were heated to 37 °C for 3 min and reactions stopped by adding 1 ml of ice-cold H-buffer. Bead-cell conjugates were briefly centrifuged in a cooled microcentrifuge and resuspended in 1 ml of ice-cold H-buffer containing complete mini EDTA-free protease inhibitor mixture tablets (Roche Applied Science), and cells were lysed by nitrogen cavitation at 4 °C. Beads containing activated or control plasma membrane fragments were retrieved using a magnet and washed with ice-cold phosphate-buffered saline. A total of 10 individual immunoisolations, each from $5 \times 10^7$ cells, were performed for both conditions and pooled.

*Prefractionation and Digestion*—Immunoisolated material from control and activated cells was combined and released from magnetic beads by boiling in denaturing Laemmli buffer, and proteins were separated by SDS-PAGE. After Coomassie Brilliant Blue staining, gel lanes were divided into 10 horizontal strips of equal size that were processed separately. Gel strips were cut into 1-$mm^3$ cubes and destained with 30% acetonitrile in 25 mM ammonium bicarbonate. Proteins were reduced with 10 mM dithiothreitol for 30 min at room temperature, alkylated with 55 mM iodoacetamide for 30 min in the dark at room temperature, and digested overnight at 37 °C with 12.5 ng/μl proteomics grade trypsin (Sigma) in 25 mM ammonium bicarbonate. Peptides were desalted on in-house manufactured reverse-phase tips, consisting of a plug of C18 matrix (3 M, Empore) packed into a pipette tip. Samples were acidified to 1% trifluoroacetic acid and tips pre-wetted and acidified with 100% methanol and 0.5% acetic acid, respectively, prior to application. Tips were washed with 0.5% acetic acid and peptides eluted with 0.1% trifluoroacetic acid in 60% acetonitrile and lyophilized in a vacuum concentrator. Lyophilized peptides were resuspended in 0.1% TFA and analyzed by LC-MS/MS.

*Mass Spectrometry*—Mass spectrometry (MS) data were acquired on an Orbitrap mass spectrometer (ThermoElectron) fitted with a nanospray ion source (Proxeon) coupled to a U3000 nanoHPLC system (Dionex). An analytical column was prepared by packing a Picotip spray emitter (150 mm length, 100 μm internal diameter, New Objective) with ProntoSIL C18 phase matrix (120-Å pore size, 3-μm bead size, Bischoff Chromatography). Mobile phase A consisted of water, 5% acetonitrile, and 0.1% formic acid, and mobile phase B consisted of acetonitrile and 0.1% formic acid. Samples were loaded onto the column at a flow rate of 700 nl/min and resolved using a 120-min gradient at a flow rate of 300 nl/min. The Orbitrap was run in a data-dependent acquisition mode in which the Orbitrap resolution was set at 60,000, and the top five multiply charged species in the 400–2000 *m/z* were selected for MS/MS. The automatic gain control for the Orbitrap was set to 500,000 ions, and the automatic gain control for the MS/MS in the ion trap was set at 10,000 ions. Three MS/MS microscans for each precursor were accumulated. Maximum injection time into the ion trap in MS/MS was 200 ms, and maximum accumulation time in the OrbiTrap was 500 ms. Three MS/MS microscans were accumulated for each precursor. Dynamic exclusion was switched on, and selected ions were excluded for 180 s before they could be selected for another round of MS/MS. Samples were injected in triplicate with exclusion lists generated from preceding runs.

*Data Analysis*—Raw MS data files were imported into MaxQuant (13) for quantitation. Most parameters were kept at their default values. Peptide False Discovery Rate was kept at 0.01 and protein False Discovery Rate at 0.01. Unique and razor peptides were used to calculate protein ratios, and a minimum of one unique peptide ratio was allowed to be used for calculation of protein ratios. Minimum peptide length was

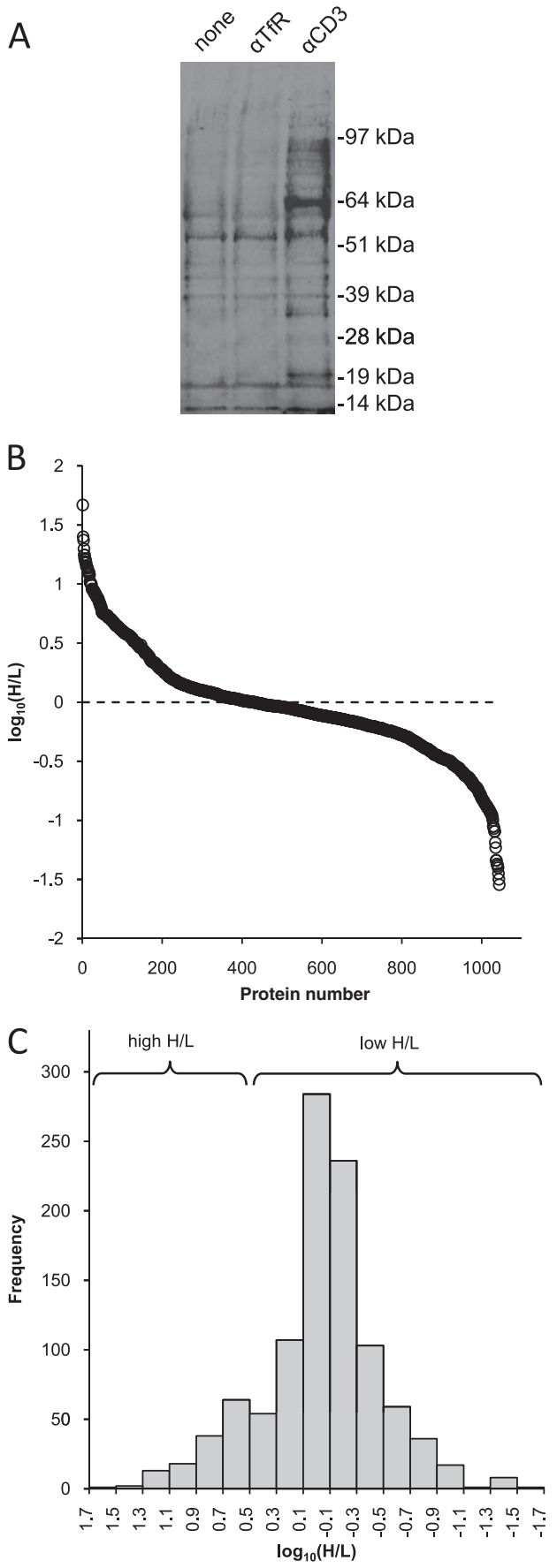


kept at six amino acids. MS/MS spectra were searched against version 3.63 of the IPI human data base. Arg-10 and Lys-8 were designated as heavy labels, methionine oxidation and N-terminal acetylation as variable modifications, and carbamidomethylation as a fixed modification. MaxQuant output data files were further analyzed using Microsoft Excel and ProteinCentre (Proxeon Biosystems).

## RESULTS

To comprehensively characterize the proteome of TCR activation sites, we used a well established procedure to isolate native plasma membrane fragments that harbor TCR signaling domains (12) in conjunction with SILAC and mass spectrometry (14). Magnetic beads coated with αCD3 antibodies were conjugated to SILAC-labeled Jurkat leukemic T cells at 0 °C, and TCR signaling was induced by warming to 37 °C for 3 min. Bead-cell conjugates were mechanically homogenized by nitrogen cavitation, and plasma membrane fragments harboring TCR-proximal signaling complexes were recovered with a magnet. As a comparative control, we used immunoisolation with αTfR (anti-transferrin receptor antibody)-coated beads. These controls were previously characterized by quantitative Western blots and shown to produce plasma membrane fragments of similar homogeneity and yield as αCD3 immunoisolations and to be depleted of active TCR signaling machinery (9, 15). Moreover, Western blots of whole Jurkat cells, conjugated with αTfR beads, showed no detectable changes in tyrosine phosphorylation compared with untreated Jurkat cells, whereas αCD3-coated positive control beads strongly induced tyrosine phosphorylations (Fig. 1*A*). This provides further validation for the use of αTfR immunoisolates as comparative negative controls. Heavy isotope (H)-labeled αCD3 immunoisolates and unlabeled light (L) αTfR immunoisolates were pooled, separated by SDS-PAGE, and subjected to in-gel trypsin digestion. More than 1500 proteins were identified by mass spectrometry. Using MaxQuant software (13), H/L ratios were assigned to more than 1000 proteins, reporting on their enrichment in TCR-activated αCD3 immunoisolates relative to the control, αTfR immunoisolates (supplemental Table 1). Normalized H/L ratios ranged from ~30 ($10^{1.5}$) to ~0.03 ($10^{-1.5}$), were $\log_{10}$-transformed to account for the ratiometric data, and graphed as a value-ordered plot and histogram (Fig. 1, *B* and *C*). The histogram showed a bimodal distribution with the major population (mode ~0), containing most of the identified proteins, occurring in equal amounts in αCD3 and αTfR immunoiso-

FIGURE 1. **A distinct proteome of αCD3 immunoisolates.** *A*, Western blot of Jurkat protein with αPiY mAb PY99 shows that αCD3 beads efficiently induce tyrosine phosphorylations following a 3-min 37 °C incubation, whereas no detectable tyrosine phosphorylations are induced by αTfR beads compared with untreated cells. *B*, value-ordered plot of $\log_{10}$-transformed H/L values assigned to more than 1000 identified proteins in immunoisolates. *C*, *histogram* showing the frequency of $\log_{10}$-transformed H/L ratios binned symmetrically around 0 in 0.2 intervals with a range from 1.7 to −1.7. A major peak around log(H/L) = 0 represents proteins equally recovered in both immunoisolates, and a second peak around log(H/L) of 0.5 signifies a sizable number of proteins that are preferentially recovered in αCD3 immunoisolates. Two proteomic populations are defined with log(H/L) > 0.5 as the "high H/L" population and one with proteins log(H/L) < 0.5 as "low H/L."

lates. Notably, a second, higher H/L population with a mode ~0.6 (H/L ~4) is clearly distinguishable. The dataset was separated into high and low H/L populations. The high H/L population ($\log_{10}$(H/L) >0.5, corresponding to H/L >3.16) contained 136 proteins and covered the majority of proteins that were specifically enriched in αCD3 immunoisolates. The second low H/L population ($\log_{10}$(H/L) <0.5) contained 909 protein identifications and included proteins recovered equally in αTfR and αCD3 immunoisolates, as well as those that were preferentially recovered in αTfR immunoisolates. In the following, we present a selected set of identified proteins and outline their implications for propagation, balancing, and attenuation of T cell activation responses, and the T cell architecture relative to TCR activation sites.

*Propagation of Plasma Membrane-proximal TCR Signals*—In line with earlier Western blot analyses (9), the data indicated a strong relative enrichment of the cytosolic protein-tyrosine kinase ZAP-70 (#3, H/L: 25.09) in αCD3 immunoisolates. The number sign indicates the position of the protein in the H/L value-sorted list of identified proteins (supplemental Table 1). Activated ZAP-70 phosphorylates tyrosines of the transmembrane scaffolding protein LAT (8). Consequently, the adaptor protein GRB2 and the signaling enzyme PLCγ associate with tyrosine-phosphorylated LAT via their SH2 protein domains, and our data confirmed the enrichment of both GRB2 (#9, H/L: 15.45) and PLCγ (#12, H/L: 14.06). Previous Western blots showed the presence of LAT in both immunoisolates (9, 10) and revealed that anchoring of GRB2 and PLCγ in αCD3 immunoisolates critically depended on enrichment of tyrosine-phosphorylated LAT in the vicinity of activated TCR (9, 10). LAT itself was not identified in this proteomic analysis, possibly because trypsin cleavage did not produce suitable LAT peptides for our analyses by mass spectrometry. However, strong relative enrichment of GRB2 (#9, H/L: 15.45) and PLCγ (#12, H/L: 14.06) strongly indicated the presence of tyrosine-phosphorylated LAT in αCD3 immunoisolates used in this study (9, 10). These results validated high H/L proteins as being specifically anchored in the proximity of activated TCR.

ProteinCenter software (Proxeon Bioinformatics A/S) was used to assign identified proteins to the "T cell receptor signaling pathway" (hsa04660) in the Kyoto Encyclopedia of Genes and Genomes (KEGG, available on line). With the exception of CD40L, all protein identifications annotated to hsa04660 were assigned an H/L value and are shown in Fig. 2*A*, documenting the strong representation of TCR-proximal signaling proteins in immunoisolates. Fig. 2*B* shows the positions of these proteins in the H/L value-sorted proteomic list, except for the identified TCR/CD3 subunits themselves that are shown in Fig. 5*A*. Eight TCR-proximal signaling proteins were strongly enriched in the αCD3 proteome with H/L values larger than eight (Fig. 2*B*). Rac small GTPase isoforms (#102, #151, H/L: 4.01, 2.82) and IL-2-inducible tyrosine kinase (ITK) (#169, H/L: 2.43) also enriched in αCD3 immunoisolates, albeit less prominently. In line with earlier observations by Western blot, the membrane-anchored src family tyrosine kinases, LCK (#470, H/L: 0.93) and FYN (#507, H/L: 0.90), were detected in equal amounts in αTfR and αCD3 immunoisolates (9). Other TCR signaling membrane-anchored proteins, cdc42 (#312, H/L: 1.23), NRas (#436, H/L: 0.99), and the cytosolic phosphatase calcineurin (#464, H/L: 0.94), were also detected in the peak of proteins recovered equally in both immunoisolates.

The proteomic data identified several proteins enriched in αCD3 immunoisolated TCR signaling plasma membrane domains that link to T cell biological activities relating to the formation of the IS. VAV3 and VAV1 isoforms (#13, #85, H/L: 13.74, 4.48) that bind SLP76 (#32, H/L: 8.33) (16) and Rap guanine nucleotide exchange factor 1/C3G (#66, H/L: 5.21) that binds CRK (#2, H/L: 45.63) and GRB2 (#9, H/L: 15.45) (17, 18) were identified as preferentially anchored in the αCD3 immunoisolates. VAV proteins and C3G act as GDP/GTP exchange factors (GEFs) for small GTPases. GEF activity of VAV proteins activates the Rac family GTPases, which in turn induce dynamic actin rearrangements downstream of TCR activation (19). Activated Rap-GTP generated by activity of the Rap GEF, C3G, was shown to drive cell spreading and "inside-out" activation of integrins such as LFA-1 and VLA-4, allowing them to avidly bind their ligands following immunoreceptor activation (20–23).

*Balancing TCR Signaling Reactions*—Besides these positive mediators of TCR activation responses, several proteins with presumed balancing functions by negative regulation of signaling reactions were enriched in the αCD3 immunoisolates. These included C-terminal src kinase (CSK, #15, H/L: 13.02), which negatively regulates LCK and FYN kinase activity (24). GTPase-activating proteins (GAPs) counteract GEF-mediated activation of small GTPases. The GTPase-activating protein for the Arf/Rho Ras family proteins, CENTD2 (#5, H/L: 19.83) (25), strongly accumulated in αCD3 immunoisolates. In contrast, IQGAP (#620, H/L: 0.75), which targets Rho family GTPases, did not enrich in the αCD3 immunoisolates, consistent with fluorescence microscopy studies showing IQGAP's relative depletion from the central regions of the IS between a CTL and a target cell (4). The tyrosine phosphatase PTPN23 (#4, H/L: 23.51) was another potential negative regulator that accumulated in αCD3 immunoisolates. The specific anchoring of balancing signaling molecules in TCR signaling plasma membrane domains has not been described previously.

*Attenuation of TCR Signaling by Endocytosis*—To attenuate signaling, activated LAT·TCR complexes are tagged for endocytosis and lysosomal degradation by ubiquitylation, which is catalyzed by CBL ubiquitin ligase (#10, #16, H/L: 15.09, 12.78) (26). Particularly noteworthy is the strong accumulation of the CBL-binding protein CIN85 (#6, H/L: 17.59) (27) in αCD3 immunoisolates. The high H/L population of the proteome also harbored two components of the ESCRT-III complex, CHMP4B (#7, H/L: 16.41) and ALIX (#8, H/L: 16.25), that mediate sorting of ubiquitylated cell surface receptors from early endosomes into the degradative endocytic pathway (28, 29). Isoforms of the ubiquitin-binding adaptor protein EPS15 (#34, H/L: 8.25) were also implicated in routing ubiquitylated EGF receptor into and along the endocytic pathway to lysosomes (30). Cell biological activities of these proteins in endocytic sorting machineries have been characterized in detail.

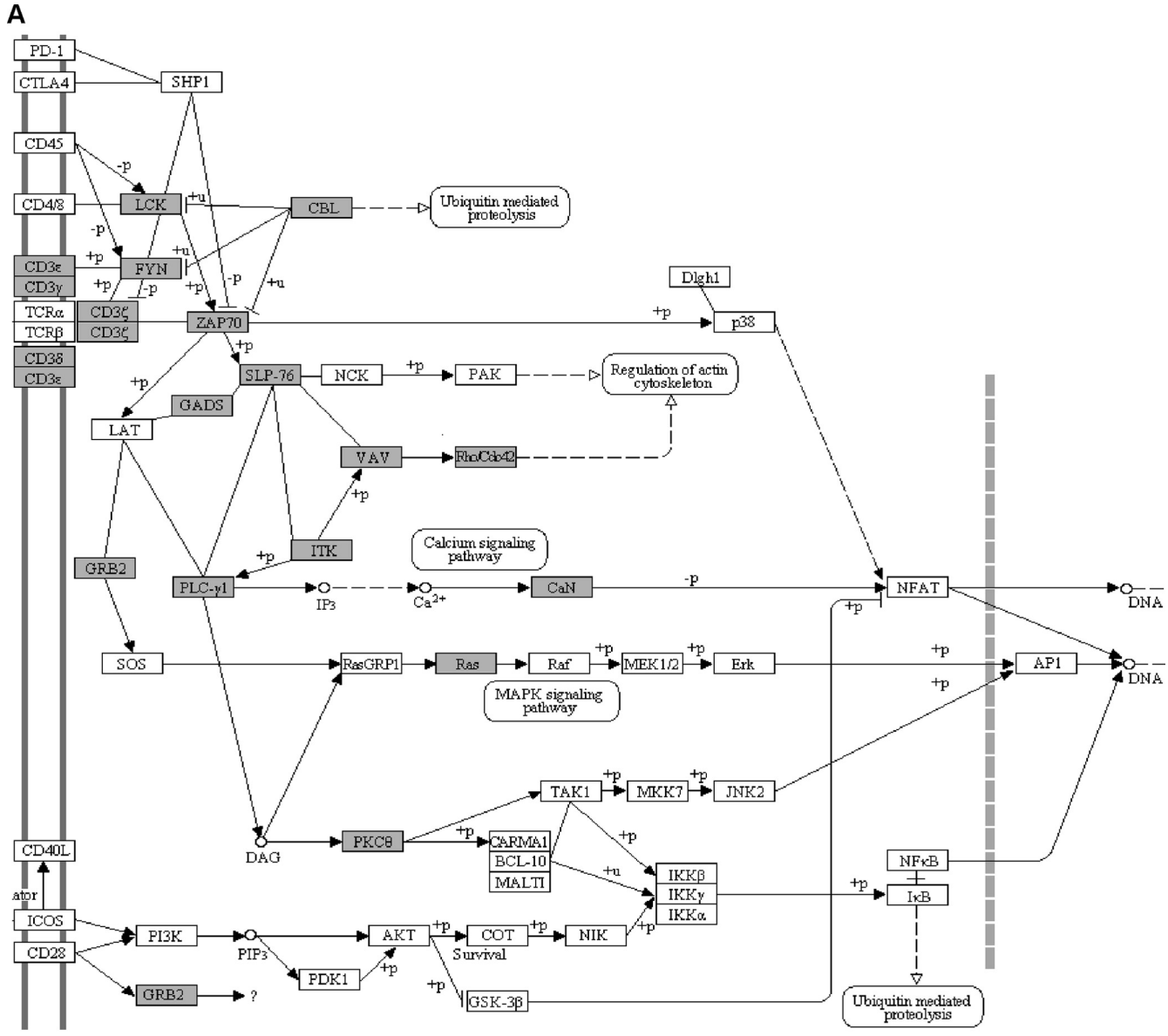
A
PD-1
CTLA4
SHP1
CD45
CD4/8
LCK
CBL
Ubiquitin mediated proteolysis
CD3ε
CD3γ
FYN
TCRα
TCRβ
CD3ζ
CD3ζ
ZAP70
Dlgh1
p38
CD3δ
CD3ε
SLP-76
NCK
PAK
Regulation of actin cytoskeleton
GADS
LAT
VAV
RhoCdc42
ITK
Calcium signaling pathway
GRB2
PLC-γ1
IP3
Ca2+
CaN
NFAT
DNA
SOS
RasGRP1
Ras
Raf
MEK1/2
Erk
AP1
DNA
MAPK signaling pathway
TAK1
MKK7
JNK2
CD40L
DAG
PKCθ
CARMA1
BCL-10
MALT1
IKKβ
IKKγ
IKKα
NFκB
IκB
ICOS
PI3K
PIP3
AKT
COT
NIK
Survival
CD28
GRB2
?
PDK1
GSK-3β
Ubiquitin mediated proteolysis
B
ZAP-70 , GRB2,
CBL, PLCγ, VAV,
GADS, PKCθ, SLP76
Rac
ITK
LCK
FYN
calcineurin
cdc42
NRas
log10(H/L)
Protein number
C
Percentage of population
PH
SH2
SH3
14/3/3
protein domain

Elucidating their specific function in the context of TCR signal transduction complexes encompasses careful characterization of their molecular anchoring mechanism and its consequences for downstream T cell activities. Such approaches can be taken as generalized strategy for any functional analysis of specific protein anchoring in T cell activation plasma membrane domains.

*Protein Domains Connecting TCR Signaling Protein Networks*—We assessed the prevalence of protein domains that mediate connections in plasma membrane TCR signaling protein complexes in the high and low H/L populations (Fig. 1*B*). Protein domains were assigned to proteome populations according to annotations in the Pfam data base. Proteins harboring SH2, SH3, pleckstrin homology, and 14-3-3 protein domains were preferentially identified in the high H/L population (Fig. 2*C*). Phosphotyrosine-SH2 domain interactions are essential for establishing the LAT-nucleated TCR signaling complexes that are recovered in αCD3 immunoisolates (10). Interaction of SH3 domains with proline-rich target motifs on signaling proteins presents another crucial connection within signaling protein networks (31). Furthermore, in activated T lymphocytes, cytosolic signaling proteins interact with the plasma membrane via pleckstrin homology domains, which bind to lipid headgroups of phosphoinositides (32). It should be noted, however, that the tightly regulated balance of D3-phosphoinositides is perturbed in Jurkat leukemic T cells due to a deficiency in the D3-phosphoinositide phosphatase PTEN (33). Multiple phosphoprotein-mediated processes are regulated by 14-3-3 proteins that bind to serine/threonine-phosphorylated proteins (34). A list of the number and percentage of identified proteins with annotated protein domains in each population according to the Pfam data base is shown in supplemental Table 2.

We performed Western blots of immunoisolates to confirm relative accumulation of tyrosine-phosphorylated protein networks at isolated TCR signaling domains (Fig. 3*A*). A Western blot of tyrosine-phosphorylated proteins shows a prominent band at 36 kDa matching electrophoretic mobility of phosphotyrosine LAT, shown to enrich in αCD3 immunoisolates (Fig. 3*B*) (9). These blots also independently verified strong relative enrichment of CRK (#2, H/L: 46. 64, Fig. 3*C*) and ALIX (#8, H/L: 16.25, Fig. 3*D*) in αCD3 immunoisolates.

*Cytoplasmic T Cell Architecture Relative to TCR Signaling Sites*—The proteins of constitutive physical complexes are recovered together in the respective immunoisolates and are therefore expected to have similar H/L ratios in this analysis. This is exemplified by MHC class I (#480, H/L: 0.93) and bound $\beta_2$-microglobulin (#452, H/L: 0.96) that are paired in the H/L-sorted proteomic list as well as by clustering of five subunits of the T-complex protein 1 between positions 213 and 243, with H/L ratios ranging from 1.71 to 1.45 (Fig. 4*A*). These observations further support the reliability of the

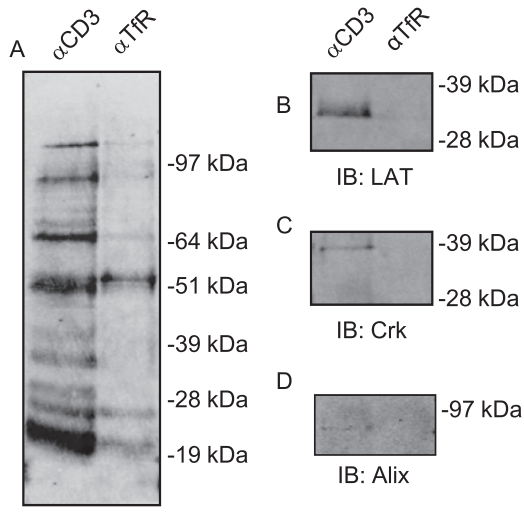


FIGURE 3. **Accumulation of tyrosine-phosphorylated protein networks at isolated TCR signaling domains.** *A,* Western blot with αPiY mAb PY99 shows strong enrichment of tyrosine-phosphorylated proteins in αCD3 immunoisolates relative to αTfR immunoisolates. These blots also confirmed relative enrichment of LAT (*B*), CRK (*C*), and ALIX (*D*) in αCD3 immunoisolates. *IB*, immunoblot.

SILAC methodology for assessing the relative enrichment of proteins in the respective immunoisolates. Notably, all identified proteins that are components of cytoplasmic ribosomes were grouped at high H/L values spreading between 8.29 and 2.00 in separate but overlapping groups of the 40 S (26 identified proteins) and 60 S (34 identified proteins) ribosomal proteins (Fig. 4*A*).

Actin filaments and microtubules play crucial and distinctive roles in T cell activation and subsequent effector functions. We therefore document the position of identified actin and tubulin in the H/L-sorted proteome (Fig. 4*B*). α- and β-tubulins are paired in the H/L-sorted proteomic list at #86 and #101 with respective H/Ls of 4.44 and 4.01 showing their accumulation in αCD3 immunoisolates, whereas γ-tubulin was not identified. In contrast, actin subunits α, γ, and β cluster at the positions 884, 888, and 914 with respective H/Ls of 0.359, 0.357, and 0.325 indicating a relative depletion of actin from αCD3 immunoisolated TCR signaling domains.

The arrangement of T cell architecture toward activation sites is reflected in the specific proteome associated with immunoisolated TCR signaling plasma membrane domains. The molecular requirements and mechanisms behind the rearrangements of the cytoskeleton relative to T cell activation sites are under intense current investigation, and the present proteomic data provide possible indications toward their further characterizations.

*Plasma Membrane Proteins*—The H/L ratio of plasma membrane proteins reports their lateral distribution in the plasma membrane relative to activated CD3 or the transferrin receptor (Fig. 5*A*). As expected, the bait proteins used for im-

FIGURE 2. **A molecular network of TCR signaling proteins in αCD3 immunoisolates.** *A,* assignment of identified proteins according to the T cell receptor signaling pathway (hsa04660) in the KEGG Pathways database. All proteins that matched identified proteins are marked by *gray boxes*, and proteins not identified are shown in *white boxes*, except for the identified CD40L protein, which was not assigned an H/L value. *B,* positions in the H/L-sorted proteomic list of the identified proteins in hsa04660 omitting the positions of TCR/CD3 subunits that are documented in Fig. 4*A*. *C,* percentage of the proteins identified in the high H/L (■) or low H/L (□) populations harboring domains with a well defined contribution to the formation of signaling protein complexes at the plasma membrane.

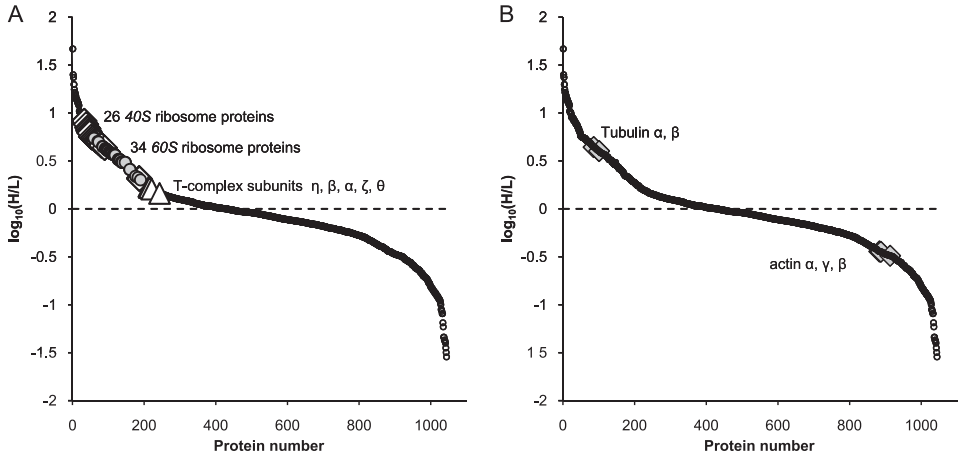


FIGURE 4. **T cell architecture reflected in the H/L sorted proteome.** *A,* grouping of proteins forming physical complexes in the H/L sorted proteomic list. 40 S (*diamonds*) and 60 S (*circles*) cytoplasmic ribosomal proteins are grouped in separate but overlapping clusters at high H/S regions. *Triangles* mark the positions of five proteins of the T complex protein 1 in the H/L sorted proteome. *B,* position of cytoskeletal proteins in the H/L sorted proteome. Tubulin subunits $\alpha$ and $\beta$ are paired in the proteomic list at high H/L values whereas $\alpha$-, $\gamma$-, and $\beta$-actin are clustered at low H/L regions.

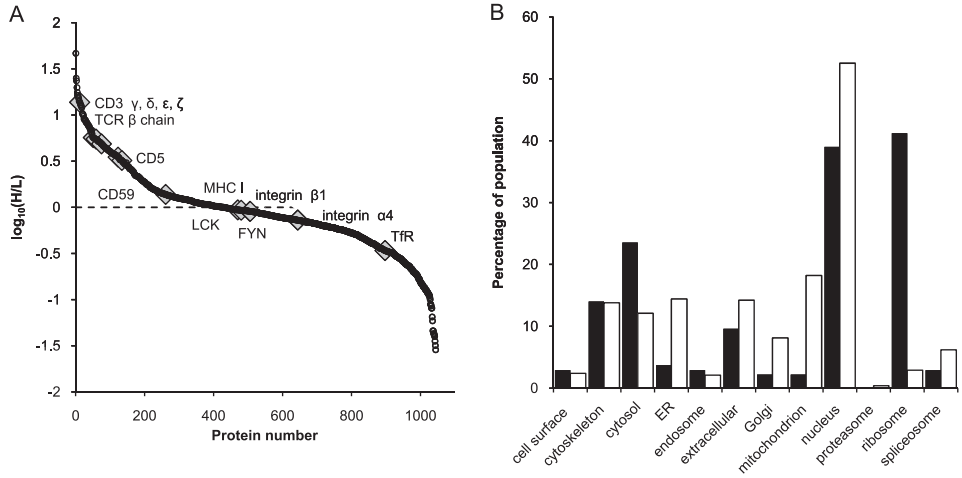


FIGURE 5. **Subcellular distribution of immunoisolated proteins.** *A,* positions of selected plasma membrane proteins along the H/L sorted proteome. *B,* percentage of proteins of the high H/L (■) and low H/L (□) populations annotated to specific subcellular compartments according to the gene ontology data base.

munoisolation, CD3·TCR complex (H/L ratios 13.54 to 3.50) and the transferrin receptor (#897, H/L: 0.34), are positioned at high and low H/L values, respectively. CD5 (#134, H/L: 3.22) also accumulated in $\alpha$CD3 immunoisolates, whereas the transmembrane protein, MHC class I (#480, H/L: 0.93), and the VLA-4 integrin subunits, $\beta$1 (#506, H/L: 0.90) and $\alpha$4 (#644, H/L: 0.73), were identified near H/L values reporting an equal recovery in both immunoisolates. The H/L value of the glycosylphosphatidylinositol-anchored protein, CD59 (#261, H/L: 1.39), in cholesterol/sphingolipid-rich membrane rafts is discussed.

*Annotation of the αCD3 Proteome to Cellular Compartments*—Proteins found in the high and low H/L proteome populations were assigned to cellular compartments according to Gene Ontology (GO) categories (Fig. 5*B*). The fraction of proteins assigned to the endoplasmic reticulum, extracellular, Golgi, mitochondria, nucleus, proteasome, and spliceosome compartments in the high H/L population was substantially smaller than that of the low H/L population, identifying no molecular links of these compartments to TCR signaling plasma membrane domains. $\alpha$CD3 immunoisolates enrich TCR/CD3 and CD5 plasma membrane proteins and the ESCRT-III endocytic sorting machinery. Consistently, a similar percentage of proteins of the high H/L population was assigned to the "cell surface" and "endosomes" GO categories relative to the low H/L population. The specific anchoring of cytoplasmic ribosomes in the $\alpha$CD3 immunoisolates is reflected in the dramatically higher percentage of identified proteins annotated to the "ribosome" GO category in the high H/L population. A high fraction of the identified proteins in the high H/L population annotated to the "cytosol" GO category, excluding the ribosomal proteins, documents the substantial anchoring of nonribosomal cytosolic proteins at TCR signaling plasma membrane domains.

It should be noted that the percentage of proteins assigned to the various cellular compartments does not reflect the quantitative recovery of these compartments in the immunoisolates. Previous quantitative Western blots showed an ~50-fold depletion of the endoplasmic reticulum and an ~100-fold depletion of mitochondria over plasma membrane in both immunoisolates (15). Nevertheless, this analysis

showed that proteins accumulating in αCD3 immunoisolates were assigned to specific cell compartments emphasizing the range of defined cellular functions associated with TCR signaling plasma membrane domains.

## DISCUSSION

Here, we present the first proteomic characterization of an isolated physical network of cell surface receptor signaling proteins anchored in its native plasma membrane lipid bilayer platform. The TCR-proximal signaling proteins assemble at the T cell plasma membrane and form signaling microclusters by lateral concatenation of protein domains of LAT and TCR transmembrane proteins (35). *In vitro* reconstitution of phosphotyrosine-LAT-nucleated signaling protein complexes on liposomes highlighted the critical contribution of the supporting lipid bilayer and its composition to LAT-nucleated cytoplasmic signaling protein networks (36). Hence, preservation of a native plasma membrane lipid bilayer platform by the αCD3 immunoisolation protocol is critical for a systematic biochemical characterization of plasma membrane-proximal TCR signaling protein complexes. Quantitative mass spectrometry of αCD3 immunoisolates and control αTfR immunoisolates allowed us to sort the identified proteins according to their specific anchoring in immunoisolated TCR signaling plasma membrane.

In addition to identifying molecular machineries involved in propagation, balancing, and attenuation of TCR signaling reactions, the αCD3 proteome mirrors the rearrangements of T cell architecture relative to TCR signaling plasma membrane domains. First, the accumulation of α- and β-tubulin in αCD3 immunoisolates correlates with the specific polarization of T cell microtubules toward TCR activation sites in Jurkat cells (6) and toward the IS between a CTL and a target cell (4). The relative depletion of actin subunits from αCD3 immunoisolates is in line with a loss of actin filaments at Jurkat TCR signaling clusters following a 3-min activation on αCD3-coated coverslips (5). This indicates that TCR signaling clusters are recovered in αCD3 immunoisolates separately from the actin-rich ring that surrounds TCR activation regions.

Moreover, our analysis indicated a selective anchoring of cytoplasmic ribosomes at TCR activation sites, and the molecular mechanism and its functional implications in T cell activation responses will be important to elucidate. It is noteworthy that the relative accumulation of cytoplasmic ribosomes in the αCD3 proteome did not correlate with the accumulation of endoplasmic reticulum membrane markers like calnexin (#612, H/L: 0.76), suggesting that ribosomes that accumulate in the αCD3 immunoisolated proteome are mainly cytosolic and are not associated with the rough endoplasmic reticulum.

High H/L values of cytosolic proteins reflect their specific anchoring in isolated TCR signaling plasma membrane domains and concomitant depletion from αTfR immunoisolates. In contrast, relative enrichment of plasma membrane-anchored molecules is measured against the background present in both immunoisolated plasma membrane fragments (15). This could explain why retardation and trapping of LCK at TCR signaling clusters, which was observed by live video microscopy (37, 38), was not resolved by previous Western blots (9) or by SILAC/mass spectrometry in this study. The H/L value of the glycosylphosphatidylinositol-anchored protein CD59 (#261, H/L: 1.39) also does not significantly report on its relative enrichment in αCD3 immunoisolates. Thus, the putative dynamic membrane raft-dependent interaction of CD59 with cholesterol/sphingolipid-rich TCR activation domains (15, 39) could not be resolved.

In primary T lymphocytes, TCR signal transduction microclusters that form in the plasma membrane following TCR triggering by cognate pMHC ligands were shown to lose active ZAP-70 2–5 min post-formation. This correlated with reduced phosphorylation of ZAP-70 target tyrosines on the LAT in the clusters (1). GRB2 and the PLCγ that bind phosphotyrosine-LAT remained associated with the αCD3 immunoisolates from Jurkat cells over a time course of 7 min (10). Thus, activation of Jurkat leukemic T cells by αCD3 antibody-coated beads used in this study does not recapitulate this important mechanism of early TCR signal regulation in T lymphocytes. This emphasizes that the molecular composition of protein networks associated with signaling plasma membrane domains will depend on the T cell type, the times of activation, the different modes of ligand presentation, and the specific defects in regulation of TCR signaling. Along these lines, the present proteomic approach maps out a general strategy for a systematic characterization of plasma membrane-proximal T cell activation responses.

*Acknowledgments—We thank the proteomics facility at the Sir William Dunn School of Pathology, under the guidance of Benjamin Thomas and with Gabriela Ridlova and David Trudgian, for obtaining proteomic data. Initial characterization of the proteome of αCD3 immunoisolated TCR signaling domains was performed with Juri Rappsilber (Wellcome Trust Centre for Cell Biology, Edinburgh, Scotland, United Kingdom). We thank Marion Brown and Neil Barclay (Sir William Dunn School of Pathology, University of Oxford) for critically reading the manuscript.*

## REFERENCES

1. Campi, G., Varma, R., and Dustin, M. L. (2005) *J. Exp. Med.* **202,** 1031–1036
2. Varma, R., Campi, G., Yokosuka, T., Saito, T., and Dustin, M. L. (2006) *Immunity* **25,** 117–127
3. Huppa, J. B., and Davis, M. M. (2003) *Nat. Rev. Immunol.* **3,** 973–983
4. Stinchcombe, J. C., Majorovits, E., Bossi, G., Fuller, S., and Griffiths, G. M. (2006) *Nature* **443,** 462–465
5. Bunnell, S. C., Kapoor, V., Trible, R. P., Zhang, W., and Samelson, L. E. (2001) *Immunity* **14,** 315–329
6. Lowin-Kropf, B., Shapiro, V. S., and Weiss, A. (1998) *J. Cell Biol.* **140,** 861–871
7. Kane, L. P., Lin, J., and Weiss, A. (2000) *Curr. Opin. Immunol.* **12,** 242–249
8. Zhang, W., Sloan-Lancaster, J., Kitchen, J., Trible, R. P., and Samelson, L. E. (1998) *Cell* **92,** 83–92
9. Harder, T., and Kuhn, M. (2000) *J. Cell Biol.* **151,** 199–208
10. Hartgroves, L. C., Lin, J., Langen, H., Zech, T., Weiss, A., and Harder, T. (2003) *J. Biol. Chem.* **278,** 20389–20394
11. Walther, T. C., and Mann, M. (2010) *J. Cell Biol.* **190,** 491–500
12. Harder, T., and Kuhn, M. (2001) *Science's Signal Transduction Knowledge Environment, stke.sciencemag.org/cgi/content/full/*

*OC_sigtrans;2001/71/pl1*
13. Cox, J., and Mann, M. (2008) *Nat. Biotechnol.* **26,** 1367–1372
14. Ong, S. E., Foster, L. J., and Mann, M. (2003) *Methods* **29,** 124–130
15. Zech, T., Ejsing, C. S., Gaus, K., de Wet, B., Shevchenko, A., Simons, K., and Harder, T. (2009) *EMBO J.* **28,** 466–476
16. Tuosto, L., Michel, F., and Acuto, O. (1996) *J. Exp. Med.* **184,** 1161–1166
17. Matsuda, M., Hashimoto, Y., Muroya, K., Hasegawa, H., Kurata, T., Tanaka, S., Nakamura, S., and Hattori, S. (1994) *Mol. Cell. Biol.* **14,** 5495–5500
18. Tanaka, S., Morishita, T., Hashimoto, Y., Hattori, S., Nakamura, S., Shibuya, M., Matuoka, K., Takenawa, T., Kurata, T., Nagashima, K., *et al.* (1994) *Proc. Natl. Acad. Sci. U.S.A.* **91,** 3443–3447
19. Tybulewicz, V. L. (2005) *Curr. Opin. Immunol.* **17,** 267–274
20. Nolz, J. C., Nacusi, L. P., Segovis, C. M., Medeiros, R. B., Mitchell, J. S., Shimizu, Y., and Billadeau, D. D. (2008) *J. Cell Biol.* **182,** 1231–1244
21. Reedquist, K. A., Ross, E., Koop, E. A., Wolthuis, R. M., Zwartkruis, F. J., van Kooyk, Y., Salmon, M., Buckley, C. D., and Bos, J. L. (2000) *J. Cell Biol.* **148,** 1151–1158
22. Lin, K. B., Freeman, S. A., Zabetian, S., Brugger, H., Weber, M., Lei, V., Dang-Lawson, M., Tse, K. W., Santamaria, R., Batista, F. D., and Gold, M. R. (2008) *Immunity* **28,** 75–87
23. Boettner, B., and Van Aelst, L. (2009) *Curr. Opin. Cell Biol.* **21,** 684–693
24. Palacios, E. H., and Weiss, A. (2004) *Oncogene* **23,** 7990–8000
25. Hawadle, M. A., Folarin, N., Martin, R., and Jackson, T. R. (2002) *Biol. Res.* **35,** 247–265
26. Balagopalan, L., Barr, V. A., Sommers, C. L., Barda-Saad, M., Goyal, A., Isakowitz, M. S., and Samelson, L. E. (2007) *Mol. Cell. Biol.* **27,** 8622–8636
27. Dikic, I. (2002) *FEBS Lett.* **529,** 110–115
28. Matsuo, H., Chevallier, J., Mayran, N., Le Blanc, I., Ferguson, C., Fauré, J., Blanc, N. S., Matile, S., Dubochet, J., Sadoul, R., Parton, R. G., Vilbois, F., and Gruenberg, J. (2004) *Science* **303,** 531–534
29. Raiborg, C., and Stenmark, H. (2009) *Nature* **458,** 445–452
30. van Bergen En Henegouwen, P. M. (2009) *Cell Commun. Signal.* **7,** 24
31. Schlessinger, J. (1994) *Curr. Opin. Genet. Dev.* **4,** 25–30
32. Lemmon, M. A. (2008) *Nat. Rev. Mol. Cell Biol.* **9,** 99–111
33. Shan, X., Czar, M. J., Bunnell, S. C., Liu, P., Liu, Y., Schwartzberg, P. L., and Wange, R. L. (2000) *Mol. Cell. Biol.* **20,** 6945–6957
34. Yaffe, M. B. (2002) *FEBS Lett.* **513,** 53–57
35. Lillemeier, B. F., Mörtelmaier, M. A., Forstner, M. B., Huppa, J. B., Groves, J. T., and Davis, M. M. (2010) *Nat. Immunol.* **11,** 90–96
36. Sangani, D., Venien-Bryan, C., and Harder, T. (2009) *Mol. Membr. Biol.* **26,** 159–170
37. Douglass, A. D., and Vale, R. D. (2005) *Cell* **121,** 937–950
38. Ike, H., Kosugi, A., Kato, A., Iino, R., Hirano, H., Fujiwara, T., Ritchie, K., and Kusumi, A. (2003) *ChemPhysChem.* **4,** 620–626
39. Lingwood, D., and Simons, K. (2010) *Science* **327,** 46–50